Local Adhesion of Membranes to Striped Surface Domains

Thomas R. Weikl† and Reinhard Lipowsky*,‡

MPI für Kolloid-und Grenzflächenforschung, Am Mühlenberg, 14476 Golm, Germany

Received May 23, 2000. In Final Form: July 31, 2000

Flexible membranes which adhere to a substrate surface along striped surface domains were theoretically studied using a "superposition" approach and Monte Carlo (MC) simulations. In the "superposition" approach, the fluctuation-induced repulsion between the membrane and the nonadhesive surface domains was approximately taken into account as a local potential. A detailed comparison of this superposition approach and the MC data shows that the strength of the fluctuation-induced potential depends *both* on the boundary conditions *and* on the physical quantity under consideration and, thus, must be viewed as a fit parameter. The shape of the adhering membrane which consists of unbound membrane arches between bound membrane segments is accessible to experiments using, for example, reflection interference microscopy.

Introduction

When dissolved in water, lipid bilayers and other biomimetic membranes form a large variety of structures in which the membranes experience mutual interactions, such as multilamellar vesicles, oriented bunches and stacks, and "myelin structures" consisting of multilamellar cylinders. In addition, these membranes can adhere to a macroscopic interface such as the container wall or the water−air interface.

There are several experimental methods by which one can probe the adhesion of such a membrane to another surface: (i) With the surface force apparatus, one can measure the direct interaction between two rigid bilayers which have been immobilized onto mica surfaces (see, for example, ref 1); (ii) the cohesion of two membranes can be controlled by micropipet aspiration. In this case, the flexibility of the membranes can be changed by varying the lateral tension (see, for example, ref 2); and (iii) the adhesion of one flexible membrane to a solid surface can be studied by reflection interference microscopy (see, for example, ref 3.

From the theoretical point of view, the interactions which control these adhesion phenomena are governed by the interplay of direct interactions arising from the forces between the molecules and of the loss of entropy arising from the steric hindrance of the two surfaces. This interplay was first studied by Helfrich using simple scaling arguments.[4] A systematic theory was developed by Lipowsky and Leibler using renormalization group methods.[5] In addition, much information on the adhesion of laterally homogeneous membranes has been obtained by Monte Carlo (MC) simulations.[6−9]

Recent work on membrane adhesion has focused on the interaction of laterally inhomogeneous systems. Examples are the adhesion of membranes via anchored stickers,[10−14] membranes with junctions,[15] the interactions of membranes which are subject to a laser trap and to an external pressure,[16−18] or the adhesion of membranes to topologically rough or stepped surfaces.[19,20]

In this article, we are concerned with the adhesion of membranes to laterally structured or imprinted surfaces which contain some adhesive domains. Such structured surfaces can be produced by a variety of experimental methods such as elastomer stamps (see, for example, refs 21 and 22); vapor deposition through grids (see, for example, ref 23); photolithography of amphiphilic monolayers (see, for example, ref 24); lithography with colloid monolayers;[25] atomic beams modulated by light masks;[26] microphase separation in diblock copolymer films;[27] or deposition of polymeric micelles.[28]

Thus, imagine a lipid bilayer or another biomimetic membrane adjacent to an imprinted surface. This surface consists of two types of domains which attract and repel the membrane, respectively. The membrane will then assume a laterally nonuniform state consisting of bound and unbound segments. We will focus here on the situation

* To whom correspondence should be addressed.
† E-mail: weikl@mpikg-golm.mpg.de.
‡ E-mail: lipowsky@mpikg-golm.mpg.de.

(1) Horn, R. *Biophys. Acta* **1984**, *778*, 224.
(2) Evans, E. *Biophys. J.* **1980**, *31*, 425.
(3) Rädler, J.; Sackmann, E. *J. Phys. II* **1993**, *3*, 727.
(4) Helfrich, W. *Z. Naturforsch.* **1978**, *33a*, 305.
(5) Lipowsky, R.; Leibler, S. *Phys. Rev. Lett.* **1986**, *56*, 2541.
(6) Gompper, G.; Kroll, D. *Europhys. Lett.* **1989**, *9*, 59.
(7) Lipowsky, R.; Zielinska, B. *Phys. Rev. Lett.* **1989**, *62*, 1572.
(8) Janke, W.; Kleinert, H.; Meinhart, M. *Phys. Lett. B* **1989**, *217*, 525.
(9) Netz, R. R.; Lipowsky, R. *Europhys. Lett.* **1995**, *29*(4), 345.
(10) Lipowsky, R. *Phys. Rev. Lett.* **1996**, *77*, 1652.
(11) Nardi, J.; Feder, T.; Bruinsma, R.; Sackmann, E. *Europhys. Lett.* **1997**, *37*, 371.
(12) Albersdörfer, A.; Feder, T.; Sackmann, E. *Biophys. J.* **1997**, *73*, 245.
(13) Weikl, T.; Netz, R.; Lipowsky, R. *Phys. Rev. E.* **2000**, *62*, 45.
(14) Komura, S.; Andelman, D. To be published.
(15) Bruinsma, R.; Goulian, M.; Pincus, P. *Biophys. J.* **1994**, *67*, 746.
(16) Bar-Ziv, R.; Menes, R.; Moses, E.; Safran, S. A. *Phys. Rev. Lett.* **1995**, *75*, 3356.
(17) (a) Menes, R.; Safran, S. A. *Phys. Rev. E* **1997**, *56*, 1891. (b) Menes, R.; Safran, S. A.; Kessler, D. *Europhys. Lett.* **1997**, *40*(2), 225.
(18) Hiergeist, C. Ph.d. Thesis, University of Potsdam, 1997.
(19) Braun, D.; Fromherz, P. *Phys. Rev. Lett.* **1998**, *81*(23), 5241.
(20) Swain, P.; Andelman, D. *Langmuir* **1999**, *15*, 8902.
(21) Drelich, J.; Miller, J. D.; Kumar, A.; Whitesides, G. M. *Colloids Surf. A* **1994**, *93*, 1.
(22) Morhard, F.; Schumacher, J.; Lenenbach, A.; Wilhelm, T.; Dahint, R.; Grunze, M.; Everhart, D. S. *Electrochem. Soc. Proc.* **1997**, *97*, 1058.
(23) Herminghaus, S.; Fery, A.; Reim, D. *Ultramicroscopy* **1997**, *69*, 211.
(24) Möller, G.; Harke, M.; Motschmann, H. *Chem. Phys. Lett.* **1997**, *0*, 0.
(25) Burmeister, F.; Schäfle, C.; Matthes, T.; Böhmisch, M.; Boneberg, J.; Leiderer, P. *Langmuir* **1997**, *13*, 2983.
(26) Drodofsky, U.; Stuhler, J.; Schulze, T.; Drewsen, M.; Brezger, B.; Pfau, T.; Mlynek, J. *Appl. Phys. B* **1997**, *65*, 755.
(27) Heier, J.; Kramer, E. J.; Walheim, S.; Krausch, G. *Macromolecules* **1997**, *30*, 6610.
(28) Spatz, J. P.; Eibeck, P.; Mössmer, S.; Möller, M.; Karmarenko, E. Y.; Khalatur, P. G.; Potemkin, I. I.; Khokhlov, A. R. *Macromolecules* **2000**, *33*, 150.

10.1021/la000708r CCC: $19.00
Published on Web 10/12/2000

in which the attractive surface domains are *strongly* attractive, and the bound membrane segments are essentially immobilized on top of these surface domains. What remains to be determined is the shape of the unbound membrane segments adjacent to the nonadhesive surface domains.

In this article, we will consider a particularly simple geometry consisting of a lattice of parallel, adhesive stripes. We will first study this system using a self-consistent or "superposition" method in which the effects of the shape fluctuations are incorporated approximately using an effective fluctuation-induced potential. To estimate the quality of this approximation, we also perform extensive MC simulations for the same problem. A detailed comparison of the self-consistent calculation and the MC data shows that there is no unique fluctuation-induced potential. Instead, the strength of this potential depends *both* on the boundary conditions *and* on the physical quantity under consideration and must be viewed as a fit parameter.

Superposition Approach

Adhesion to Laterally Homogeneous Surfaces. For laterally homogeneous systems, the effect of the shape fluctuations has often been treated in an approximate way using an entropic or fluctuation-induced potential. For a membrane adjacent to another surface or wall, the latter potential has the general form $V_{\rm fl} = c_{\rm fl}T^2/2\kappa l^2$ as originally proposed by Helfrich,[4] where T denotes the temperature in energy units,[29] κ the bending rigidity of the membrane, and l is the mean separation between membrane and surface.

In a more systematic treatment, this entropically induced interaction arises from the renormalization of the hard wall interaction.[5] Its strength, which is governed by the dimensionless coefficient $c_{\rm fl}$, depends on the boundary conditions used to confine the membranes.[10] The value of $c_{\rm fl}$ has been determined by MC simulations and was found to vary from $c_{\rm fl} \simeq 0.08$ for a single membrane between parallel walls[6] to $c_{\rm fl} = 0.115 \pm 0.005$ for a membrane subject to an external pressure.[7,9,10]

In the latter case, the membrane is pushed by an external pressure, P, toward a hard wall, and the entropic or fluctuation-induced potential $V_{\rm fl}$ has a well-defined meaning: it is *defined* in such a way that the mean separation follows from $-\partial V_{\rm fl}(l)/\partial l = P$. It must be emphasized, however, that this potential is defined only with respect to this *specific* physical observable.

In general, the interpretation of the entropic or fluctuation-induced interaction is subtle even for laterally homogeneous systems. First, in the presence of attractive van der Waals interactions, a simple superposition of the latter interactions and the fluctuation-induced interactions is not correct, as first pointed out in ref 5. Second, the fluctuation-induced interaction is often derived using a collision picture in which the membrane is envisaged to undergo frequent collisions with the other surface. The latter picture is also incorrect as shown by an explicit calculation of the contact probabilities.[30] Finally, there is no reason to believe that the fluctuation-induced potential defined via $-\partial V_{\rm fl}(l)/\partial l = P$ will apply to other quantities such as the free energy or the correlation length.

All of the limitations of the superposition approach just reviewed for the case of laterally homogeneous systems should also apply to laterally inhomogeneous or nonuniform systems as discussed next.

Adhesion to Laterally Inhomogeneous Surfaces. First, we will describe the partition function which we would like to calculate in order to determine the shape of the membrane which is attracted to some adhesive surface domains. In the absence of lateral tension, thermal fluctuations of fluid membranes are governed by their bending elasticity. In the Monge parametrization, the configurations of the membrane are described by the displacement field $l(x,y)$ which measures the local separation of the membrane from the substrate. As usual, x and y denote Cartesian coordinates in the plane of the substrate. For an oriented membrane, the Hamiltonian has the generic form

$$H\{l\} = \int \mathrm{d}x\, \mathrm{d}y\, \frac{\kappa}{2}(\nabla^2 l)^2 \qquad (1)$$

where κ is the bending rigidity as before. For two interacting membranes with separation field l and bending rigidities κ_1 and κ_2, the symbol κ denotes the effective bending rigidity $\kappa = \kappa_1\kappa_2/(\kappa_1 + \kappa_2)$. The partition function Z of the system is the functional integral over all possible membrane configurations weighted with the Boltzmann factor $\exp[-H\{l\}/T]$:

$$Z = \int' Dl(x,y) \mathrm{e}^{-\mathrm{H}\{l\}/T} \qquad (2)$$

The prime at the integral sign indicates that the functional integral is restricted to positive separation fields $l(x,y)$ and to configurations which satisfy the boundary conditions imposed by the strong adhesive surface domains to which the membrane is attached. Because of these restrictions, an explicit analytical evaluation of the partition function Z and the free energy $F = -T \ln Z$ becomes untractable.

Within the superposition approach, the effect of the thermal membrane fluctuations is now taken into account as a local repulsive potential added to the bending energy which leads to the free energy functional

$$\Delta F\{l\} = \int \mathrm{d}x\, \mathrm{d}y \left[\frac{\kappa}{2}(\nabla^2 l)^2 + \frac{c_{\rm fl}T^2}{2\kappa l^2}\right] \qquad (3)$$

The differential equation for the shape profile $\bar{l} = \bar{l}(x,y)$ is obtained from the first variation, $\partial(\Delta F) = 0$, of this free energy functional (see Appendix A). As a result, one obtains the Euler−Lagrange equation:

$$\kappa\nabla^4 l = \frac{c_{\rm fl}T^2}{\kappa l^3} \qquad (4)$$

which has to be supplemented by a suitable set of boundary conditions for l at the pinning sites. An estimate for the free energy is achieved by inserting the solution $l = \bar{l}$ of eq4 back into eq 3:

$$\Delta F = \int \mathrm{d}x\, \mathrm{d}y \left[\frac{\kappa}{2}(\nabla^2 \bar{l})^2 + \frac{c_{\rm fl}T^2}{2\kappa \bar{l}^2}\right] \qquad (5)$$

Precisely speaking, ΔF is a free energy difference with respect to the flat state $\bar{l} = l_o$ at large pinning distances l_o (see below).

The superposition approach just described has been previously used for membranes which are subject to an external pressure which acts to push the membrane

(29) The temperature T in energy units corresponds to $k_{\rm B}T'$ where T' is the temperature in Kelvin and $k_{\rm B}$ denotes Boltzmann's constant.

(30) Hiergeist, C.; Lipowsky, R. *Physica A* **1997**, *244*, 164.

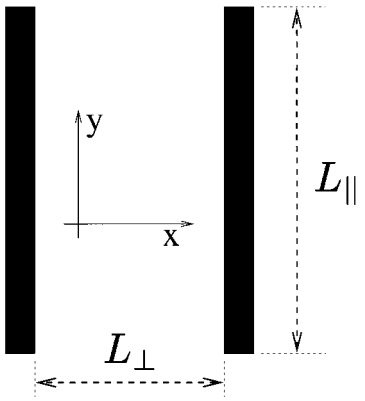

Figure 1. Two types of surface domains: Strongly adhesive stripes (black) and repulsive surface domains (white). The length of the adhesive stripes is denoted by $L_{||}$, their distance is denoted by $L_\perp$.

toward the wall.[17,18] Here, we will study the membrane behavior in the absence of such a pressure, which eliminates one parameter from the problem and leads to shape profiles which exhibit some universal features.

Specific Geometry: Parallel Contact Lines. We will now focus on a particularly simple geometry which consists of parallel stripes as shown in Figure 1. The length of these stripes is denoted by $L_{||}$ and the distance between the stripes is denoted by $L_\perp$.

The stripes represent adhesive surface domains prepared, for example, by a monolayer of adhesive or sticky molecules. The surface domains between the stripes, on the other hand, are nonadhesive and exert a purely repulsive hard wall interaction onto the membrane. As a consequence, the membrane will assume a laterally nonuniform state consisting of bound and unbound segments adjacent to the adhesive and nonadhesive surface domains, respectively.

We focus on the situation of strongly adhesive stripes which essentially immobilize the membrane at a small, uniform separation l_o from the substrate surface. Between these strongly bound segments, the membrane is unbound because it is pushed away from the nonadhesive surface domains by thermally-excited shape fluctuations. These unbound segments will be characterized by an average shape profile $\bar{l} = \bar{l}(x,y)$, which represents the local separation of the membrane from the nonadhesive surface domains. In general, the local separation $\bar{l}(x,y)$ will exceed the separation l_o from the adhesive stripes and will increase with the lateral distance x from those stripes. An equivalent geometry is provided by a pair of membranes which are pinned together at striped domains.

We now apply the superposition approach to this specific geometry. If the parallel length $L_{||}$ of the adhesive stripes is much larger than the stripe distance $L_\perp$ (see Figure 1) we can assume translational symmetry in the y-direction parallel to the stripes. The difference free energy of the superposition approach, eq 5, then can be written as

$$\Delta F = L_{||} \int_0^{L_\perp} \mathrm{d}x \left[\frac{\kappa}{2} \left(\frac{\partial^2 \bar{l}}{\partial x^2} \right)^2 + \frac{c_{\mathrm{fl}} T^2}{2\kappa \bar{l}^2} \right] \tag{6}$$

and the Euler−Lagrange eq 4 reads

$$\kappa \frac{\partial^4 \bar{l}}{\partial x^4} = \frac{c_{\mathrm{fl}} T^2}{\kappa \bar{l}^3} \tag{7}$$

with a shape profile $\bar{l} = \bar{l}(x)$, which only depends on the coordinate x. Because of the fixed membrane distance $\bar{l} = l_o$ along the contact lines of the membranes, the boundary conditions at $x = 0$ and $x = L_\perp$ are given by

$$\bar{l}|_{x=0} = \bar{l}|_{x=L_\perp} = l_o \tag{8}$$

and

$$\left. \frac{\partial \bar{l}}{\partial x} \right|_{x=0} = \left. \frac{\partial \bar{l}}{\partial x} \right|_{x=L_\perp} = 0 \tag{9}$$

The second boundary condition, eq 9, is necessary in order to have a finite contact curvature. The shape profile $\bar{l}(x)$ is determined by the Euler−Lagrange eq 7 and the boundary conditions are determined by eqs 8 and 9. For large l_o, and thus for large $\bar{l}$, the fluctuation potential in eq 6 declines to zero, and the solution of the Euler−Lagrange eq 7 at the conditions in eqs 8 and 9 is the flat membrane state with constant shape profile $\bar{l}(x) = l_o$. Equation 6 gives the free energy difference with respect to this flat state described by the profile $\bar{l}(x) = l_o$ which is achieved for large l_o.

Because of the reflection symmetry of the membrane with respect to $x = L_\perp/2$, it is sufficient to consider only one-half of the membrane between the adhesive stripes. For this purpose, we need two boundary conditions at $x = L_\perp/2$. These boundary conditions follow directly from the smoothness of the membrane and the symmetry at $x = L_\perp/2$ and are given by

$$\left. \frac{\partial \bar{l}}{\partial x} \right|_{x=L_\perp/2} = 0 \quad \text{and} \quad \left. \frac{\partial^3 \bar{l}}{\partial x^3} \right|_{x=L_\perp/2} = 0 \tag{10}$$

It is interesting to note that the second boundary condition in eq 10 also follows from the minimization of the free energy with respect to the value $l_{\max} \equiv l(L_\perp/2)$ of the separation at the position of the symmetry plane (see Appendix A). For a reduction of the parameters and a simplification of the notation, it is convenient to introduce the rescaled shape profile

$$\zeta(x) = c_{\mathrm{fl}}^{-1/4}\, \bar{l}(x) \sqrt{\kappa/T} \tag{11}$$

The Euler−Lagrange eq 7 then can be written in the form

$$\frac{\partial^4 \zeta}{\partial x^4} = \frac{1}{\zeta^3} \tag{12}$$

and the difference free energy (eq 6) reads:

$$\Delta F = L_{||} T \sqrt{c_{\mathrm{fl}}} \int_0^{L_\perp/2} \mathrm{d}x \left[\left(\frac{\partial^2 \zeta}{\partial x^2} \right)^2 + \frac{1}{\zeta^2} \right] \tag{13}$$

The boundary conditions for $\zeta(x)$ at $x = 0$ and $x = L_\perp/2$ are

$$\zeta(0) = c_{\mathrm{fl}}^{-1/4} l_o \sqrt{\frac{\kappa}{T}} \equiv \zeta_o, \quad \left. \frac{\partial \zeta}{\partial x} \right|_{x=0} = 0 \tag{14}$$

$$\left. \frac{\partial \zeta}{\partial x} \right|_{x=L_\perp/2} = 0, \quad \left. \frac{\partial^3 \zeta}{\partial x^3} \right|_{x=L_\perp/2} = 0 \tag{15}$$

At first sight, the problem seems to depend on the two parameters ζ_o and $L_\perp$, which enter via the integral in eq 13 and the boundary conditions in eqs 14 and 15.

However, the difference free energy (eq 13) is invariant under the scale transformation

$$(L_{||}, L_{\perp}, \zeta_o) \rightarrow (bL_{||}, bL_{\perp}, b\zeta_o) \tag{16}$$

because the shape profile ζ, which is the solution of the Euler−Lagrange eq 12 with the boundary conditions in eqs 14 and 15, scales as $(x,\zeta) \rightarrow (bx, b\zeta)$. So we have

$$\frac{\Delta F}{T\sqrt{c_{\mathrm{fl}}}} = L_{||}\,\hat{f}\,(L_{\perp},\zeta_o) = bL_{||}\,\hat{f}\,(bL_{\perp}, b\zeta_o) \tag{17}$$

and with the choice $b = 1/\zeta_o$ for the scaling factor b, i.e., by taking the rescaled contact separation ζ_o as the unit length scale, the difference free energy can be written as

$$\frac{\Delta F}{T\sqrt{c_{\mathrm{fl}}}} = \frac{L_{||}}{\zeta_o}\,\hat{f}\left(\frac{L_{\perp}}{\zeta_o}, 1\right) \equiv \frac{L_{||}}{\zeta_o}\Phi_1\left(\frac{L_{\perp}}{\zeta_o}\right) \tag{18}$$

With $b = 1/L_{\perp}$, the stripe distance $L_{\perp}$ is taken as the unit length scale which leads to

$$\frac{\Delta F}{T\sqrt{c_{\mathrm{fl}}}} = \frac{L_{||}}{L_{\perp}}\,\hat{f}\left(1, \frac{\zeta_o}{L_{\perp}}\right) \equiv \frac{L_{||}}{L_{\perp}}\Phi_2\left(\frac{\zeta_o}{L_{\perp}}\right) \tag{19}$$

Thus, the relevant parameter turns out to be the ratio $L_{\perp}/\zeta_o$ of the stripe distance $L_{\perp}$ and the rescaled contact separation ζ_o. The difference free energy (eq 13) is essentially determined by the function $\Phi_1(L_{\perp}/\zeta_o)$ in the case where ζ_o is taken as the unit length scale, and by $\Phi_2(\zeta_o/L_{\perp})$ when $L_{\perp}$ is considered as the unit length. According to eqs 18 and 19, the functions Φ_1 and Φ_2 are related via

$$\Phi_1\left(\frac{L_{\perp}}{\zeta_o}\right) = \frac{\zeta_o}{L_{\perp}}\Phi_2\left(\frac{\zeta_o}{L_{\perp}}\right) \tag{20}$$

Results. The numerical integration of the differential eq 12 with the boundary conditions in eqs 14 and 15 and the subsequent calculation of the difference free energy (eq 13) is carried out with a MATHEMATICA program[31] which can be found in Appendix B. The results were confirmed with MAPLE and routines of the NAG library, respectively.[32]

Shape Profiles. In Figure 2, we see numerical results of the rescaled shape profile ζ for several ratios $\zeta_o/L_{\perp}$ of the rescaled contact separation ζ_o and the stripe distance $L_{\perp}$. The shape profiles of Figure 2 show an *increase* of the maximum membrane separation $\zeta_{\max} = \zeta(L_{\perp}/2)$ with *decreasing* contact separation ζ_o for given stripe distance $L_{\perp}$. In Figure 3, the maximum separation $\zeta_{\max}$ in units of $L_{\perp}$ is displayed as a function of $L_{\perp}/\zeta_o$. Both figures demonstrate that the overall shape profile strongly depends on changes of the rescaled separation ζ_o at the boundary of the membrane.

Free Energy. It is instructive to display the difference free energy (eq 13) via both scaling functions Φ_1 and Φ_2 defined in eqs 18 and 19. In Figure 4a, we see the scaling function Φ_1 as a function of $L_{\perp}/\zeta_o$ in a double-logarithmic representation. The scaling function Φ_1, where the rescaled contact distance ζ_o was taken as the unit length scale, refers to the situation in which ζ_o and the length $L_{||}$ of the adhesive stripes are fixed, but the stripe distance

(31) *MATHEMATICA*. Wolfram Research Inc. Champaign, IL.
(32) *MAPLE*. Waterloo Maple Inc. Ontario, Canada; NAG Fortran Library (Numerical Algorithms Group, Oxford, U.K.

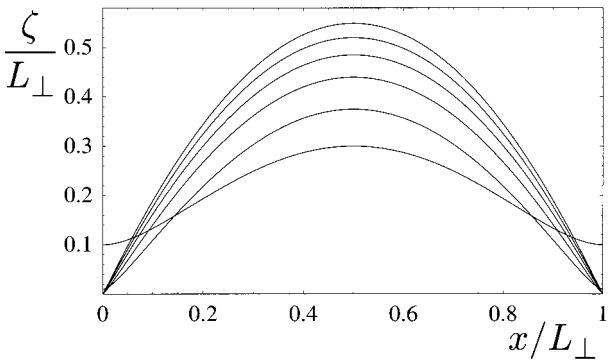

Figure 2. Rescaled shape profiles $\zeta(x)$ of the superposition approach in units of the stripe distance $L_{\perp}$. The ratio of the rescaled contact distance ζ_o and the stripe distance $L_{\perp}$ is $\zeta_o/L_{\perp} = 10^{-1}$, 10^{-2}, 10^{-3}, 10^{-4}, 10^{-5}, and 10^{-6} (center, from bottom to top),

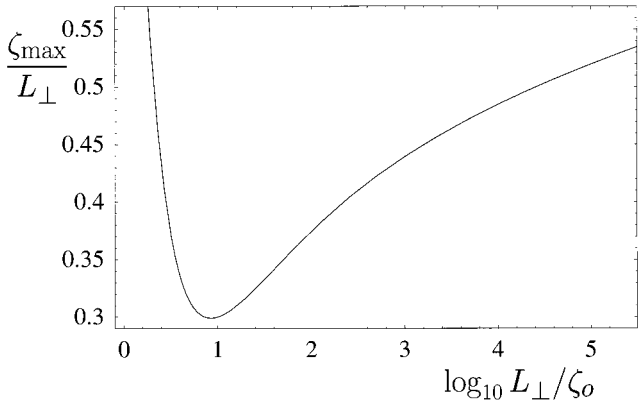

Figure 3. The rescaled maximum separation $\zeta_{\max} = \zeta(L_{\perp}/2)$ in units of the stripe distance $L_{\perp}$ as a function of the decadic logarithm of $L_{\perp}/\zeta_o$ where z_o is the rescaled contact separation.

$L_{\perp}$ can be varied. Thus, Φ_1 can be understood as a fluctuation-induced contribution to the interaction potential of the adhesive stripes. It is implicitly assumed here that the relation $L_{\perp} \ll L_{||}$ is fulfilled for all values of $L_{\perp}$.

For small values of $L_{\perp}/\zeta_o$, the function Φ_1 is linear in $L_{\perp}$. This just reflects the fact that for $L_{\perp}/\zeta_o \ll 1$, the membrane is essentially flat due to the boundary constraints. Then, only the fluctuation potential contributes to the dimensionless free energy, and from eq 13 we conclude that $\Phi_1 = L_{\perp}/(2\zeta_o)$. Note, however, that this free energy contribution of the fluctuation potential is an artifact of the superposition approach: Because of the boundary constraints, contacts between membrane and wall do not occur for $L_{\perp}/\zeta_o \ll 1$, and the fluctuation repulsion should be irrelevant. This artifact can only be overcome by taking the value $c_{\mathrm{fl}} = 0$ for the fluctuation coefficient at small $L_{\perp}/\zeta_o$. A more detailed discussion of the parameter-dependence of the effective fluctuation coefficient will be given in the next sections where we compare results from the superposition approach and from MC simulations.

It is more difficult to explain the behavior of Φ_1 for larger values of $L_{\perp}/\zeta_o$, where first a maximum is reached for $L_{\perp}/\zeta_o \approx 20$, and then Φ_1 tends to the constant value $\Phi_1 = 2.105$. The latter cannot be explained by a scale invariance of the shape profiles for large $L_{\perp}/\zeta_o$, (see Figure 2). Unfortunately, a comparison with MC data is not possible at high values of $L_{\perp}/\zeta_o$, (see below).

In Figure 4b, we see the scaling function Φ_2 which depends on $L_{\perp}/\zeta_o$. It is natural to choose Φ_2 as a representation of the difference free energy (eq 13) in

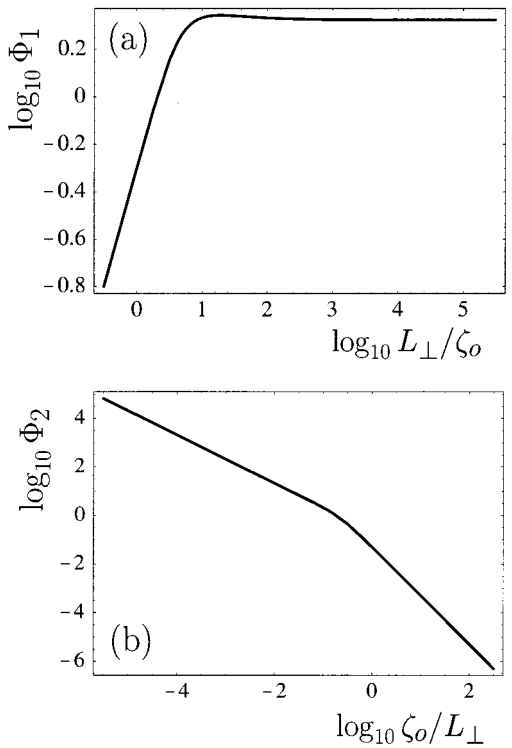

Figure 4. Double-logarithmic plot of: (a) Φ_1 as a function of the ratio $L_\perp/\zeta_o$ of the stripe distance $L_\perp$ and rescaled contact separation ζ_o; (b) Φ_2 as a function of $\zeta_o/L_\perp$. The scaling functions Φ_1 and Φ_2 are both proportional to the difference free energy ΔF (see eqs 18 and 19).

experimental situations where the distance $L_\perp$ and length $L_\parallel$ of the adhesive stripes are fixed, but the rescaled contact separation ζ_o can be varied. In accordance with eq 20 and Figure 4a, the function Φ_2 is inversely proportional to $\zeta_o/L_\perp$ at small values of $\zeta_o/L_\perp$ and scales as $\Phi_2 \sim (\zeta_o/L_\perp)^{-2}$ for large values of $\zeta_o/L_\perp$.

Monte Carlo Simulations of the Pinned Membrane

Discretization and Implementation of the Boundary Conditions. We now discuss our MC simulations for the same adhesion problem as studied in the last section, i.e., for a membrane which is irreversibly attached to a pair of parallel adhesive stripes at a contact separation l_o with respect to the plane of the substrate. For the simulations, we need a discretized distance field $l_{x,y}$, where (x,y) denotes the site of a square lattice with coordinates xa and ya, a being the lattice constant. In the MC simulations, the lattice constant a enters as a new length, compared to the superposition approach. In real membranes, this length corresponds to a molecular length, e.g., the thickness of the membrane. At the contact lines with $x = 0$ and $x = L_\perp \equiv N_\perp a$ (see Figure 1), the membrane distance is equal to l_o:

$$l_{0,y} = l_{N_\perp,y} = l_o \tag{21}$$

At $y = 0$ and $y = L_\parallel \equiv N_\parallel a$, we assume periodic boundary conditions:

$$l_{x,N_\parallel+1} = l_{x,1}; \quad l_{x,0} = l_{x,N_\parallel} \tag{22}$$

For a stripe length $L_\parallel$ with $L_\parallel \gg L_\perp$, the results of the simulation are only weakly dependent on $L_\parallel$ because the correlation lengths in the y-direction are approximately proportional to the width $L_\perp$ of the membrane stripe. The discretized Hamiltonian can be written as

$$H = \sum_{x=1}^{N_\perp-1}\sum_{y=1}^{N_\parallel}\frac{\kappa}{2a^2}(\Delta_d l_{x,y})^2 + \rho\sum_{y=1}^{N_\parallel}\frac{\kappa}{2a^2}[(l_{1,y}-l_o)^2 + (l_{N_\perp-1,y}-l_o)^2] \tag{23}$$

where the discretized Laplace operator Δ_d is given by $\Delta_d l_{x,y} = l_{x+1,y} + l_{x-1,y} + l_{x,y+1} + l_{x,y-1} - 4l_{x,y}$, and κ again denotes the bending rigidity. The term proportional to ρ reflects the contribution of the boundary sites with $x = 0$ and $y = N_\perp a$ to the bending energy because for $l_{-1,y} = l_{0,y} = l_o$ and $l_{N_\perp+1,y} = l_{N_\perp,y} = l_o$, the boundary curvatures are given by $\Delta_d l_{0,y} = l_{1,y} - l_o$ and $\Delta_d l_{N_\perp,y} = l_{N_\perp-1,y} - l_o$. In the following, we only consider one-half of the Wigner−Seitz cell around each boundary site to be part of the membrane. Thus, we take $\rho = 1/2$. In the continuum limit with large $L_\perp/a$ and l_o/a, the boundary energy term leads for positive ρ to shape profiles with vanishing boundary gradient at $x = 0$ and $L_\perp = 0$ as demanded by the boundary conditions in eq 9. For $\rho = 0$, however, boundary gradients do not contribute to the bending energy, and the Hamiltonian (eq 23) with boundary conditions (in eq 21) then corresponds to a membrane with given contact distance l_o but free boundary gradients.

Integration Method To Determine the Free Energy. Our aim is to determine the free energy difference ΔF with respect to the state with $l_o = \infty$, as well as the shape profiles as a function of the contact distance l_o or the rescaled contact distance $z_o = (l_o/a)\sqrt{\kappa/T}$ for given stripe width $L_\perp$ and length $L_\parallel \gg L_\perp$. Defining the rescaled distance field $z_{x,y} = (l_{x,y}/a)\sqrt{\kappa/T}$, the Hamiltonian (eq 23) with $\rho = 1/2$ can be written in the form

$$\frac{H}{T} = \sum_{x=1}^{N_\perp-1}\sum_{y=1}^{N_\parallel}\frac{1}{2}(\Delta_d z_{x,y})^2 + \sum_{y=1}^{N_\parallel}\frac{1}{4}[(z_{1,y}-z_o)^2 + (z_{N_\perp-1,y}-z_o)^2] \tag{24}$$

and the partition function reads

$$Z = [\prod_{x=1}^{N_\perp-1}\prod_{y=1}^{N_\parallel}\int_0^\infty \mathrm{d}l_{x,y}]\, \mathrm{e}^{-H/T} = \left(\frac{Ta^2}{\kappa}\right)^{N/2}[\prod_{x=1}^{N_\perp-1}\prod_{y=1}^{N_\parallel}\int_0^\infty \mathrm{d}z_{x,y}]\, \mathrm{e}^{-H/T} \tag{25}$$

with $N = (N_\perp - 1)N_\parallel$. A direct evaluation of partition functions by MC simulations is difficult.[33,34] We therefore study average quantities which represent derivatives of ln Z with respect to some system parameter, and determine each quantity as a function of this parameter. The partition function is then obtained by integration. A classical variant is the relation

$$\frac{\mathrm{d}\ln Z}{\mathrm{d}T} = \frac{1}{Z}\left\{[\prod_{x=1}^{N_\perp-1}\prod_{y=1}^{N_\parallel}\int_0^\infty \mathrm{d}l_{x,y}]\, \mathrm{e}^{-H/T}\frac{H}{T^2}\right\} = \left\langle\frac{H}{T^2}\right\rangle \tag{26}$$

Taking into account the temperature dependence of the rescaled contact distance $z_o = (l_o/a)\sqrt{\kappa/T}$, the integration

(33) Binder, K., Ed. *Applications of the Monte Carlo Methods in Statistical Physics*; Springer: Berlin, 1984.
(34) Allen, M. P.; Tildesley, D. J. *Computer Simulation of Liquids*; Clarendon Press: Oxford, 1987.

then leads to

$$\frac{\Delta F}{T} = -(\ln Z|_{T_1} - \ln Z|_{T_o}) = -\int_{T_o}^{T_1} \left\langle \frac{H}{T^2} \right\rangle \mathrm{d}T$$

$$= \int_{T_o}^{T_1} \frac{2}{z_o} \left\langle \frac{H}{T} \right\rangle \frac{\mathrm{d}z_o}{\mathrm{d}T} \mathrm{d}T = \int_{z_o(T_o)}^{z_o(T_1)} \frac{2}{z_o} \left\langle \frac{H}{T} \right\rangle \mathrm{d}z_o \qquad (27)$$

Thus, this approach requires the determination of the reduced internal energy $\langle H/T \rangle$.

To improve the statistics, we found it more useful to consider

$$\frac{\mathrm{d} \ln Z}{\mathrm{d}z_o} = \frac{1}{Z} \left\{ [\prod_{x=1}^{N_\perp - 1} \prod_{y=1}^{N_\parallel} \int_0^\infty \mathrm{d}l_{x,y}] \, \mathrm{e}^{-H/T} \frac{\mathrm{d}}{\mathrm{d}z_o} \left(-\frac{H}{T} \right) \right\} =$$

$$\left\langle \frac{d}{\mathrm{d}z_o} \left(-\frac{H}{T} \right) \right\rangle = \left\langle -\sum_{y=1}^{N_\parallel} (\Delta_d z_{1,y} + \Delta_d z_{N_\perp - 1,y}) + \right.$$

$$\left. \frac{1}{2} \sum_{y=1}^{N_\parallel} [(z_{1,y} - z_o) + (z_{N_\perp - 1,y} - z_o)] \right\rangle \qquad (28)$$

and integrate subsequently to obtain

$$\frac{\Delta F}{T} = -(\ln Z|_{z_o = z_{o,2}} - \ln Z|_{z_o = z_{o,1}}) = -\int_{z_{o,1}}^{z_{o,2}} \frac{\mathrm{d} \ln Z}{\mathrm{d}z_o} \mathrm{d}z_o \qquad (29)$$

If $\mathrm{d} \ln Z/\mathrm{d}z_o$ is known for sufficiently many values of the rescaled contact distance z_o, the difference of the free energies between the state with $z_o = \infty$ and a state with finite z_o can be determined by interpolation and integration. At $z_o = \infty$, the average $\mathrm{d} \ln Z/\mathrm{d}z_o$ is equal to zero, and the free energy then is invariant with respect to changes of z_o. This can also be seen from the second line of eq 28 which takes into account the symmetry of the partition function Z with respect to the plane $z = z_o$ because then the mean rescaled shape profile $\langle z_{x,y} \rangle$ is equal to z_o independent of x and y.

According to eqs 24 and 25, the partition function can be written as

$$Z = \left(\frac{Ta^2}{\kappa} \right)^{N/2} \tilde{Z}(z_o) \qquad (30)$$

where $\tilde{Z} = [\prod_{x=1}^{N_\perp - 1} \prod_{y=1}^{N_\parallel} \int_0^\infty \mathrm{d}z_{x,y}] \mathrm{e}^{-H/T}$ only depends on the rescaled contact distance $z_o = (l_o/a)\sqrt{\kappa/T}$. From this, we conclude the following considering the T-dependence of Z:

$$\left\langle \frac{H}{T} \right\rangle = T \frac{\mathrm{d} \ln Z}{\mathrm{d}T} = \frac{N}{2} + T \frac{\mathrm{d} \ln Z}{\mathrm{d}z_o} \frac{\mathrm{d}z_o}{\mathrm{d}T} = \frac{N}{2} - \frac{z_o}{2} \frac{\mathrm{d} \ln Z}{\mathrm{d}z_o} \qquad (31)$$

This equation connects the average $\langle H/T \rangle$ and $\mathrm{d} \ln Z/\mathrm{d}z_o$. At $z_o = \infty$, we have $\mathrm{d} \ln Z/\mathrm{d}z_o = 0$, and therefore $\langle H/T \rangle = N/2$ in accordance with the equipartition theorem. We also see from eq 31 that $\langle H/T \rangle$ has to be equal to $N/2$ for $z_o = 0$, too.

Results. In Figures 5 and 6, we see MC results for $\langle H/T \rangle/N$ and $(\mathrm{d} \ln Z/\mathrm{d}z_o)/N_\parallel$ as a function of the rescaled contact distance z_o for $L_\perp/a = N_\perp = 24$, 32, and 40. The data are averages from simulations with 2×10^7 MC steps per lattice site and the reduced stripe lengths $L_\parallel/a = N_\parallel = 110$, 150, and 200, respectively. The ratios of $L_\parallel/L_\perp$ are large enough to guarantee that the averages are independent of $L_\parallel$. This was checked by running simulations

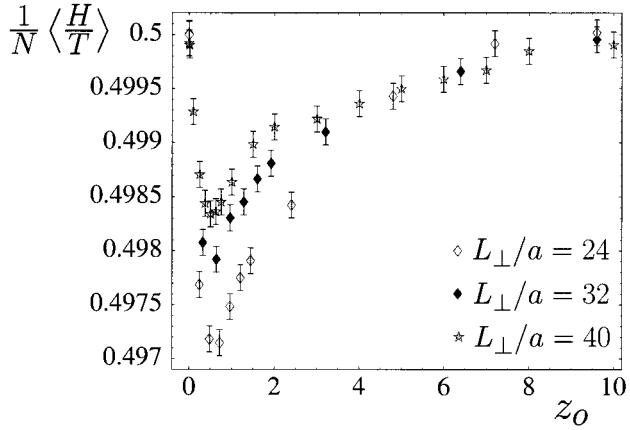

Figure 5. Monte Carlo results for the internal energy per lattice site $\langle H/T \rangle/N$ as a function of the rescale contact separation z_o for the reduced stripe distances $L_\perp/a = N_\perp = 24$, 32, and 40. The number of lattice sites is $N = (N_\perp - 1)N_\parallel$ where $N_\parallel = L_\parallel/a$ denotes the length of the adhesive stripes in units of the lattice constant a.

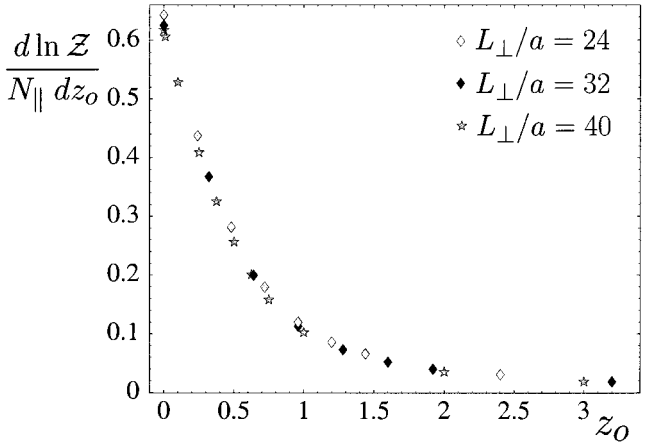

Figure 6. Monte Carlo results for $(\mathrm{d} \ln Z/\mathrm{d}z_o)/N_\parallel$ as a function of the rescaled contact separation z_o for the reduced stripe distances $L_\perp/a = 24$, 32, and 40, where Z denotes the partition function and $N_\parallel = L_\parallel/a$ is the length of the adhesive stripes in units of the lattice constant a. The statistical errors are smaller than the symbol sizes.

with different values of $L_\parallel$ as well as by measuring the correlation functions. Because the statistical errors for $(\mathrm{d} \ln Z/\mathrm{d}z_o)$ are considerably smaller than the errors of $\langle H/T \rangle$, we use the data of Figure 6 to extract the free energy ΔF through interpolation and integration according to eq 29.

The resulting free energy differences between the state with $z_o = \infty$ and states with finite z_o are shown in Figure 7. Because of the fluctuation repulsion, ΔF increases with decreasing z_o. The free energies $(L_\perp/L_\parallel)$ $(\Delta F/T)$ per quadratic stripe segment coincide at large values of $z_o a/L_\perp = z_o/N_\perp$. This is a consequence of the scale invariance of the bending energy in the continuum limit with large $L_\perp/a$ and z_o/a. In this limit, the shape profiles, the free energy and other physical quantities become independent of the lattice spacing a.

At small values of $z_o a/L_\perp$, discretization effects lead to deviations of the three curves for $L_\perp/a = 24$, 32, and 40. The discretization becomes noticeable at values of $z_o = (l_o/a)\sqrt{\kappa/T}$ around 1: first the curve for $L_\perp/a = 24$ splits off; at smaller values of $z_o a/L_\perp$ also the curves for $L_\perp/a = 32$ and 40 differ from each other. A comparison of the curves suggests that the free energy for $L_\perp/a = 40$ should be almost unaffected by the discretization until values of

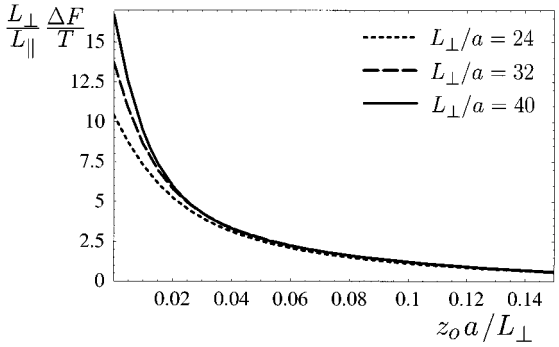

Figure 7. Dimensionless free energy $(L_\perp/L_\parallel)$ $(\Delta F/T)$ per quadratic membrane segment resulting from the interpolation of the data in Figure 6 and the subsequent integration according to eq 29. The stripe distance $L_\perp$ is given in units of the lattice constant a, the stripe length is denoted by $L_\parallel$, and z_o is the rescaled contact separation of the membrane.

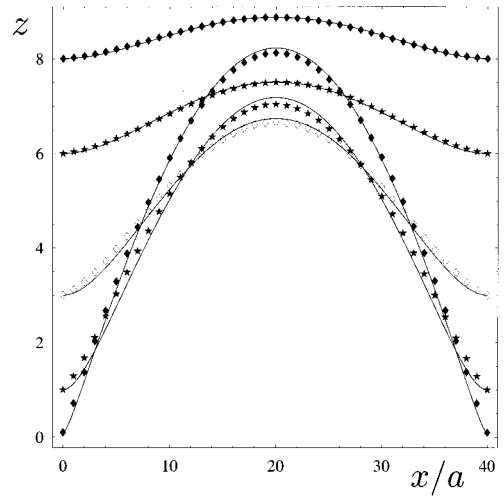

Figure 8. Comparison of rescaled shape profiles $z(x)$ from Monte Carlo simulations (data points) and from the superposition approach (lines) for the reduced stripe distance $L_\perp/a = 40$ and the rescaled contact distances $z_o = 8$, 6, 3, 1, and 0.1. The fit values of the fluctuation coefficient are $c_{fl} = 0.085$ for $z_o = 8$, $c_{fl} = 0.082$ for $z_o = 6$, $c_{fl} = 0.100$ for $z_o = 3$, $c_{fl} = 0.098$ for $z_o = 1$, and $c_{fl} = 0.071$ for $z_o = 0.1$; for a graphical representation, see Figure 9.

$z_o a/L_\perp$ around 0.02 or $L_\perp/(z_o a) \approx 50$. However, discretization effects, arising from the influence of the lattice spacing a, should not be seen as a mere numerical artifact because a corresponds to a microscopic length scale of the membrane, e.g., the membrane thickness. This microscopic length is a natural cutoff for the membrane fluctuations; on scales smaller than this cutoff, shape fluctuations are not possible.

Comparison of the two Methods

Shape Profiles. We now compare the outcome from the MC simulations with corresponding results from the superposition approach. In Figure 8, we see shape profiles for $L_\perp/a = 40$ and $z_o = 8$, 6, 3, 1, and 0.1. The data points originate from MC simulations with 2×10^7 steps per lattice site, and statistical errors are smaller than the symbol sizes. The full lines are results from the superposition approach *with values of* c_{fl} *which were fitted to the MC data* following the method of least squares. It has to be noted that the rescaled contact distances of this section, z_o, and of section 2, ζ_o, are not identical but are related by $\zeta_o = c_{fl}^{-1/4} z_o a$, where a is the lattice spacing.

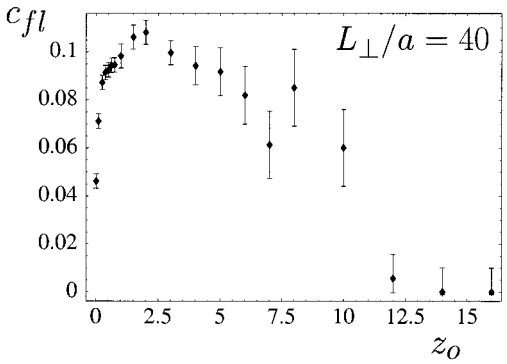

Figure 9. The fluctuation coefficient c_{fl} as obtained from fitting shape profiles of the superposition approach to Monte Carlo data for simulations with reduced stripe distance $L_\perp/a = 40$ and several values of the rescaled contact separation z_o (see also Figure 8).

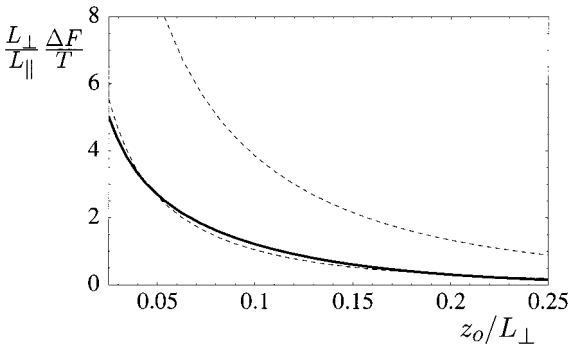

Figure 10. Comparison of the dimensionless free energy per quadratic stripe segment $(L_\perp/L_\parallel)(\Delta F/T)$ from the Monte Carlo data for the reduced stripe distance $L_\perp/a = 40$ and from the superposition approach with the fluctuation coefficients $c_{fl} = 0.115$ (upper dashed line) and $c_{fl} = 0.025$ (lower dashed line). Here, $L_\parallel$ denotes the length of the adhesive stripes, and a is the lattice constant.

The fit values are given in the caption of Figure 8 and represented graphically in Figure 9.

Using optimal values for the fluctuation coefficient c_{fl}, the agreement of the shape profiles for given z_o is rather good. This is not trivial, because the fluctuation approach implies rather crude approximations, as discussed previously. As a systematic deviation, the shape profiles from the superposition approach lie at the membrane edges below and in the membrane middle above the MC data.

In Figure 9, we see fit values for c_{fl} as a function of the rescaled contact distance z_o for $L_\perp/a = 40$. Three regimes can be distinguished: (i) At large values of z_o, collisions of the membrane with the substrate do not occur due to the fixed membrane boundaries at the adhesive stripes. The values for c_{fl} therefore rapidly decline to zero with increasing z_o. (ii) In a regime of small rescaled contact distances $z_o \lesssim 1$, the influence of the lattice spacing a of the MC simulations becomes noticeable. The superposition approach, however, is a continuum theory due to lack of a microscopic length scale, and therefore effectively contains fluctuations also on length scales smaller than a. These fluctuations lead to an additional repulsion for small z_o, compared to the MC simulations. In the naive fit of the fluctuation coefficient, this effect is corrected by a relatively small value of c_{fl}. (iii) In an intermediate regime with $1 \lesssim z_o \lesssim 4$, the values for z_o are close to 0.10 and reach a maximum.

Free Energy. A comparison of the results for the free energy difference $\Delta F = F(z_o) - F(z_o = \infty)$ can be seen in Figure 10. The full line for $(L_\perp/L_\parallel)\Delta F$ comes from an

interpolation and integration of the MC data for $d \ln Z/dz_o$ at the reduced stripe width $L_\perp/a = 40$, and the dashed lines correspond to results in the superposition approach. The upper dashed line is the free energy (eq 13) for the solution of the shape eq 12 with the boundary conditions shown in eqs 14 and 15 with $L_\perp/a = 40$, $\zeta_o = c_{fl}^{-1/4} z_o a$, and $c_{fl} = 0.115$. This value for c_{fl} has been derived from MC simulations of membranes pushed together by an external pressure, (see Introduction). For the lower dashed line, the fluctuation parameter $c_{fl} = 0.025$ has been fitted to reach optimal agreement with the MC curve in the range $1 < z_o < 10$. This fit value of c_{fl} is considerably smaller than (i) the values for average parallel membranes which range between 0.08 and 0.115 (see Introduction) and (ii) the values for c_{fl} derived from the fitting to the mean MC shape profiles which range between 0.06 and 0.11 for $1 < z_o < 10$ (see Figure 9).

Conclusion and Outlook

From these results, we conclude that there is no unique fluctuation-induced potential, i.e., no repulsive potential which applies to arbitrary boundary conditions. Instead, the coefficient c_{fl} depends on the boundary conditions arising from the pinning geometry. In this article, the coefficient c_{fl} was determined for a membrane which is locally pinned to a substrate at parallel adhesive stripes. This was achieved by a comparison with MC simulations. The geometry-dependence of the coefficient c_{fl} implies that c_{fl} is a function of different length scales, e.g. a function of the rescaled contact distance z_o for given distance $L_\perp$ of the adhesive stripes. In addition, different quantities lead to different values of c_{fl} within the superposition approach: The fit value of c_{fl} for the free energy is much smaller than the fit values for the shape profile. Similar behavior has also been observed for strings governed by lateral tension (see ref 35).

Finally, we emphasize that the membrane shape as theoretically determined here could be directly observed experimentally. As mentioned, there are several experimental methods by which one can prepare substrate surfaces with adhesive surface domains. One could then study the adhesion of vesicles to such surfaces and measure the shape profile of the membrane within the contact area using, e.g., interference contrast microscopy as in ref 3. For the stripe geometry considered here, the water pockets under the membrane arches are directly connected to the surrounding solution, which implies that they can freely adjust their volume and, thus, do not experience an (effective) pressure. Furthermore, the membrane arches will be unaffected by a lateral tension, Σ, as long as the distance $L_\perp$ between the stripes does not exceed the length scale $\sqrt{\kappa/\Sigma}$ which separates the rigidity-dominated regime from the tension-dominated one. If $L_\perp \gg \sqrt{\kappa/\Sigma}$, on the other hand, one has two different types of membrane segments: up to lateral distances $\sim\sqrt{\kappa/\Sigma}$ away from the adhesive stripes, the membrane will attain the shape profile described above; further away from the stripes, the membrane will be tense and, thus, essentially flat.

Nomenclature

a = lattice constant
b = scaling factor
c_{fl} = fluctuation coefficient
ΔF = difference free energy
ΔF = free energy functional
ϵ = variational parameter
$\hat{f}$ = scaling function
Φ_1, Φ_2 = scaling functions
H = effective Hamiltonian
κ = (effective) bending rigidity
l = separation field
$\bar{l}$ = separation profile (superposition)
l_o = contact separation
l_{max} = maximum separation $\bar{l}\,(L_\perp/2)$
$L_\parallel$ = length of the adhesive stripes
$L_\perp$ = distance of the adhesive stripes
$N_\parallel$ = reduced stripe length $L_\parallel/a$
$N_\perp$ = reduced stripe distance $L_\perp/a$
N = number of lattice sites $(N_\perp - 1)N_\parallel$
ρ = proportionality factor for the boundary energy
T = temperature in energy units
V_{fl} = fluctuation-induced potential
x, y = spatial coordinates
z = rescaled separation field $(l/a)\sqrt{\kappa/T}$ (MC simulations)
z_o = rescaled contact separation $(l_o/a)\sqrt{\kappa/T}$ (MC simulations)
ζ = rescaled separation $c_{fl}^{-1/4}\bar{l}\sqrt{\kappa/T}$ (superposition)
ζ_o = rescaled contact separation $c_{fl}^{-1/4} l_o \sqrt{\kappa/T}$ (superposition)
ζ_{max} = rescaled maximum separation $\zeta(L_\perp/2)$ (superposition)

Acknowledgment. We would like to thank G. Gompper, W. Helfrich, R. R. Netz, S. Safran, and U. Seifert for helpful discussions.

Appendix A: Variational Calculation

In this appendix, we minimize the free energy ΔF of the membrane with respect to the separation $\bar{l}_{max} = \bar{l}(L_\perp/2)$ in the middle between the two adhesive stripes. Because there are no constraints on $\bar{l}_{max}$, the equilibrium free energy ΔF is invariant under an infinitesimal displacement $\delta\bar{l}_{max}$ of $\bar{l}_{max}$. We thus consider a variation

$$\bar{l}(x) + \epsilon\cdot\delta\bar{l}(x) \tag{A1}$$

of the equilibrium profile $\bar{l}$ with

$$\delta\bar{l}(0) = \delta\bar{l}\,'(0) = \delta\bar{l}\,'(L_\perp/2) = 0, \quad \delta\bar{l}(L_\perp/2) = \delta\bar{l}_{max} \tag{A2}$$

To simplify the notation, partial derivatives with respect to x are denoted by primes and $\bar{l}$ will be simply written as l. The free energy ΔF can be written in the form

$$\Delta F = \int_0^{L_\perp/2} f(l, l', l'')\mathrm{d}x \tag{A3}$$

with

$$f = 2L_\parallel\left[\frac{\kappa}{2}(l'')^2 + \frac{c_{fl}T^2}{2\kappa l^2}\right] \tag{A4}$$

Because l is the equilibrium shape profile, we have

$$\delta(\Delta F) = \left.\frac{\mathrm{d}(\Delta F)}{\mathrm{d}\epsilon}\right|_{\epsilon=0} = \int_0^{L_\perp/2}\left[\frac{\partial f}{\partial l}\cdot\delta l + \frac{\partial f}{\partial l'}\cdot\delta l' + \frac{\partial f}{\partial l''}\cdot\delta l''\right]\mathrm{d}x = 0 \tag{A5}$$

Integrating by parts, we obtain

$$\delta(\Delta F) = \int_0^{L_\perp/2}\left[\frac{\partial f}{\partial l} - \frac{\partial}{\partial x}\frac{\partial f}{\partial l'} + \frac{\partial^2}{\partial x^2}\frac{\partial f}{\partial l''}\right]\cdot\delta l\,\mathrm{d}x + \left[\frac{\partial f}{\partial l'}\cdot\delta l + \frac{\partial f}{\partial l''}\cdot\delta l' - \frac{\partial}{\partial x}\frac{\partial f}{\partial l''}\cdot\delta l\right]_0^{L_\perp/2} \tag{A6}$$

(35) Lipowsky, R. Habilitation Thesis, LMU, München, 1987.

With eq A4, this yields

$$\delta(\Delta F) = 2L_{||}\int_0^{L_\perp/2}\left[\kappa\frac{\partial^4 l}{\partial x^4} - \frac{c_{fl}T^2}{\kappa l^3}\right]\cdot\delta l\ \mathrm{d}x + 2\kappa L_{||}[l''\cdot\delta l' - l'''\cdot\delta l]_0^{L_\perp/2} \quad \text{(A7)}$$

Because $\delta(\Delta F)$ vanishes for arbitrary variational functions δl, the equilibrium shape profile l has to fulfill the shape equation

$$\kappa\frac{\partial^4 l}{\partial x^4} = \frac{c_{fl}T^2}{\kappa l^3} \quad \text{(A8)}$$

Taking into account eq A2, we end up with

$$\delta(\Delta F) = -2\kappa L_\perp l'''(L_\perp/2)\cdot\delta l_{max} = 0 \quad \text{(A9)}$$

which is equivalent to the second boundary condition in eq 10.

Appendix B: Numerical Integration of the Euler−Lagrange Equation

In this appendix, we present a MATHEMATICA program[31] for the numerical integration of the shape eq 12 at the boundary conditions shown in eqs 14 and 15. The program is an implementation of the so-called *shooting* method: The differential eq 12 is first integrated for a complete set of four boundary conditions at $x = 0$, namely the two conditions shown in eq 14 as well as $\zeta''(0) = j(0) = p$ and $\zeta'''(0) = j'(0) = q$, then the parameters p and q are varied until the solution fulfills the two boundary conditions shown in eq 15 at $x = L_\perp/2$. For this purpose, we define the two functions "firstDerivative", $\zeta'(L_\perp/2)$, and "thirdDerivative", $\zeta'''L_\perp/2) = j'(L_\perp/2)$, depending on p and q. In the program, $L_\perp$ is simply denoted by L, and the separation ζ by z. Derivatives with respect to x are indicated by primes as in the previous appendix.

The integration of the differential equation for the four given boundary conditions at $x = 0$ is carried out with the MATHEMATICA routine "NDSolve". With the routine "FindRoot", values for p and q are determined for which the boundary conditions shown in eq 15 at $x = L_\perp/2$ are fulfilled with relative and absolute errors smaller than 10^{-6} (default error parameters of "FindRoot"). In the last line of the program, the free energy (eq 13) is calculated. The whole program is defined as a module depending on the rescaled contact distance $z_o = \zeta_o$ and the distance $L_\perp$ of the adhesive stripes. The starting values of the routine "FindRoot", however, have to be adjusted roughly to the given values of ζ_o and $L_\perp$. The shown starting values, for example, are suitable for $\zeta_o = 0.1$ and values of $L_\perp$ below 10^4. Because of the scale invariance of the free energy, it is sufficient to determine ΔF for an arbitrary value of ζ_o as a function of the ratio $L_\perp/\zeta_o$, compare eq 18.

MATHEMATICA program:

```
freeEnergy[zo_,L_]: = Module[
  {x,z,j,p,q,curve,firstDerivative,thirdDerivative,
    pqSolution,solutionCurve},

curve[p_,q_]: = NDSolve[{z''[x]==j[x],j''[x]==1/z[x]^3,
    z[0]==zo,z[0]==0,j[0]==p,j[0]==q},
    {z,j},{x,0,L/2},MaxSteps→1000];

firstDerivative[p_,q_]:=z'[L/2]/.curve[p,q][[1]];

thirdDerivative[p_,q_]:=j'[L/2]/.curve[p,q][[1]];

pqSolution = FindRoot[
    {firstDerivative[p,q]==0, thirdDerivative[p,q]==0},
    {p,0.001,0.002},{q,−0.001,−0.002},MaxIterations→100];

solutionCurve = curve[p/.pqSolution, q/.pqSolution];

NIntegrate[Evaluate[(j[x]^2 + 1/z[x]^2)/.solutionCurve][[1]],
    {x,0,L/2}]
```

LA000708R